Journal of Sound and Vibration (2001) **239**(5), 995–1012
doi:10.1006/jsvi.2000.3179, available online at http://www.idealibrary.com on IDEAL®

ASSESSMENT OF CLASSICAL NUMERICAL MODELS FOR THE SEPARATE FLUID–STRUCTURE MODAL ANALYSIS

J.-R. Cho and J.-M. Song

School of Mechanical Engineering, Pusan National University, Jangjeon-Dong, Kumjung-Ku, Pusan 609-735, *Korea*

(*Received* 22 *October* 1999, *and in final form* 5 *June* 2000)

In the numerical analysis of the eigen behavior of huge liquid-storage tanks, treatment of large-scale matrices becomes a burden owing to the hydrodynamic interaction between two different media, structure and liquid. In order to overcome such a problem, it is classical to split the dynamic system into two separate problem regions, the structure and the liquid, by utilizing the mass-adding technique. In general, the eigenbehavior of interior liquid is characterized by the sloshing mode while that of the structure by the bulging mode, and furthermore the two modes exhibit a weak coupling. Based upon this weak coupling, the structure deformation to the sloshing mode and the liquid free-surface fluctuation to the bulging mode have been neglected in the classical added-mass computation. This paper is concerned with the refinement and the assessment of classical interaction modelling by including both neglected effects. In order to estimate the accurate mass added to the structure, we refine the classical procedure by reflecting the liquid free-surface fluctuation. On the other hand, we qualitatively and quantitatively analyze the additional effect by the structure deformation onto the classical rigid-tank sloshing model. Through the numerical experiments carried out with a representative cylindrical liquid-storage tank, we illustrate our theoretical results.

1. INTRODUCTION

In the analysis of the dynamic behavior of liquid-storage tanks, the most important step is to appropriately model the hydrodynamic interaction between two different media, structure and liquid. By the way, in most cases of numerical simulations for such problems, approximations of whole state variables in governing equations for motions of the structure and the liquid end up with large-scale numerical matrix systems. To resolve such a problem, a technique called mass-adding has been widely employed in most engineering applications so that large-scale dynamic interaction problems can be reduced to two separate dynamic problems.

However, it is obvious that the reliability of constructed decoupled problems depends definitely on the accuracy of calculated added-masses. Many investigators studied the numerical techniques for calculating accurate added-masses of liquid. As a result, the basic idea of calculating added-mass is well known as follows; starting from an abstract pressure field in the liquid regions, one estimates the equivalent mass added to the structure by virtually equating the pressure force to the equivalent acceleration force acting on the structure.

Among the research on theoretical estimation of added-masses are those by Gupta [1], Chopra and Hall [2], Housner [3] and Haroun [4, 5]. On the other hand, Zienkiewicz *et al.*

0022-460X/01/050995 + 18 $35.00/0

[6], Tedesco *et al.* [7, 8] and Rajasankar *et al.* [9] presented finite element approximations for added-mass matrices. In addition, Brebbia *et al.* [10] and Khai [11] studied the application of finite and boundary element methods to the calculation of added-masses. Recently, a study on the added-mass of viscous fluids has been reported by Conca *et al.* [12].

As is widely known, the eigenbehavior of liquid-storage tanks exhibits two distinguished eigenmodes, the sloshing mode and the bulging mode. The former is related to the vertical fluctuation of the liquid free surface, while the latter characterizes the structure deformation. Since the coupling between these two modes is weak, the effect of liquid free-surface sloshing on the structure deformation and the effect of structure deformation on the liquid motion have been traditionally excluded. By excluding both the effects, the modal analysis of interaction systems can be easily separated, according to the usual mass-adding technique [4, 3, 9], i.e., the classical separate modal analysis models. The framework for fully coupled numerical formulations is well established in a book by Morand and Ohayon [13]. In the coupled formulation, while it requires complicated and expensive numerical treatment, both effects may be easily included.

In this study, we aim at the assessment of classical simplified separate interaction models by including both the neglected effects. For the added-mass matrix of the separated structure region, we refine the classical numerical procedure so that it accounts for the liquid free-surface fluctuation. With the refined procedure, we compute the spatial distributions of nodal added-masses and corresponding natural frequencies. By comparing the numerical results obtained by the classical and the refined procedures, we intend to examine the additional effect by the liquid free-surface fluctuation on the bulging mode. In addition, we derive the numerical formulation that reflects the structure deformation. With the derived numerical formulation, we estimate natural frequencies for various combinations of major problem parameters. As a model problem, we consider the horizontal eigenbehavior, in which the liquid free-surface fluctuation and the structure bending deformation are most considerable. Through the comparison of natural frequencies obtained by the classical and the present formulations, we investigate the parametric effect of structure deformation on the sloshing mode.

2. EIGENCHARACTERISTICS OF LIQUID-STORAGE TANKS

Referring to Figure 1, let us consider the horizontal eigencharacteristics (in the x direction) of a cylindrical tank containing liquid, in which the structure deformation and the liquid pressure are coupled at the liquid–structure interface. Figure 2 illustrates the dominance of two distinguished eigenmodes, the sloshing and the bulging modes, with respect to the liquid free-surface fluctuation height η along the natural frequency and the participating liquid mass portion respectively. In relatively lower-frequency range, the coupled system exhibits a dominance of the free-surface motion (i.e., the sloshing mode) while the structure deformation dominates as the natural frequency becomes higher (i.e., the bulging mode). In addition, the two modes show quite weak coupling, and hence separate dynamic analysis has been carried out for many cases. Furthermore, it has been found as depicted in Figure 2, that a certain amount of liquid m_s in the upper region takes part in the free-surface motion, while the rest of the liquid m_b contributes to the structure deformation [7, 8].

This implies that the liquid mass interacting with the structure is partial and furthermore its spatial distribution is not uniform.

From the illustration showing the frequency-wise dominance, one can infer that the effect of liquid free-surface fluctuation on the bulging mode decreases as the natural frequency

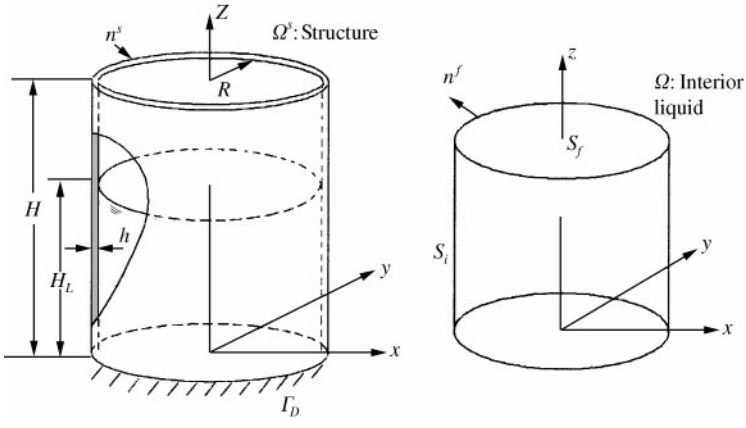

Figure 1. A liquid-storage cylindrical tank and its geometry definition.

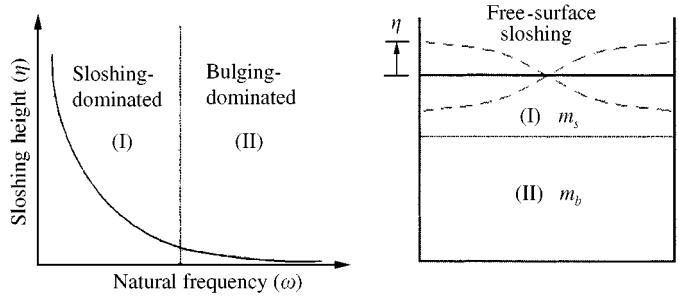

Figure 2. Frequency-wise and liquid-region-wise dominance in the eigenbehavior.

increases, while that of structure deformation on the sloshing mode increases in proportion to the increase of natural frequency. On the other hand, from the physical point of view, one can imagine that the intensity of interaction caused by both additional effects is a function of the relative stiffness of the structure to the interior liquid. Therefore, the suitability of classical interface modeling for the construction of two equivalent separate dynamic systems is frequency and problem dependent.

3. FLUID–STRUCTURE INTERACTION PROBLEM

For the theoretical analysis of fluid–structure interaction problems, let us consider a cylindrical liquid-storage tank represented in Figure 1, where $\Omega \in R^3$ deotes an open bounded fluid domain with piecewise smooth boundary $\partial\Omega = \overline{S_f \cup S_i}$. Here, S_f denotes a free surface and S_i indicates the boundary region which is in contact with the structure. A storage cylinder is defined by $\Omega_s \in R^3$ with its smooth boundary $\partial\Omega = \overline{\Gamma_D \cup \Gamma_N}$, where Γ_D is the displacement boundary region while the traction boundary region denoted by Γ_N is composed of fluid-structure interface S_i and the other parts subjected to external traction (but, we here assume no external loading).

As a preliminary step of our theoretical study, we now record two sets of field equations governing the dynamic motions of the structure and the liquid respectively.

3.1. FOR THE STRUCTURE REGION

By denoting **u** as continuous triple-vector dynamic displacement fields of the structure, we have equations governing the dynamic motion of the structure and the corresponding boundary conditions given by

$$\left.\begin{aligned} \sigma_{ij}(\mathbf{u})_{,j} - c\dot{u}_i + f_i = \rho_s \ddot{u}_i, \quad & \text{in} \quad \Omega_s \times (0, t) \\ \sigma_{ij} n_j^s = -p_i, \quad & \text{on} \quad S_i \\ u_i = 0, \quad & \text{on} \quad \Gamma_D \end{aligned}\right\}, \quad i, j = x, y, z, \tag{1}$$

where ρ_s, c and f_i are the density, damping coefficient and body force components, respectively, and σ_{ij} denote *Cauchy* stress components. Furthermore, n_j^s indicate components of outward unit vector normal to the structure and p_i are hydrodynamic pressure components (viewing **p** as a force vector in Cartesian co-ordinates) acting on the structure.

The dynamic displacement field is related to stress tensor through the generalized *Hooke*'s law and strain-displacement relations.

3.2. FOR THE LIQUID REGION

For an interior liquid, we assume that the flow is incompressible and irrotational (i.e., curl-free; $\nabla \times \mathbf{v} = \mathbf{0}$ with **v** denoted as continuous triple-vector velocity fields). Furthermore, we make an additional assumption of inviscid flow. The reader may refer to Conca *et al.* [12] for a recent analytic study on the viscous fluid–structure interaction problems. For the ideal flow, we have a velocity potential function $\varphi(\mathbf{x}; t)$ satisfying

$$\varphi(\mathbf{x}; t) : \mathbf{v} = \nabla\varphi. \tag{2}$$

Denoting the density of the interior liquid by ρ and neglecting its body force, we have *Euler* equations, the continuity equation and boundary conditions:

$$\left.\begin{aligned} \rho\dot{\mathbf{v}} = -\nabla p \\ \nabla \cdot \mathbf{v} = 0 \end{aligned}\right\}, \quad \text{in} \quad \Omega \times (0, t],$$

$$\mathbf{v} \cdot \mathbf{n}^f = \dot{\mathbf{u}} \cdot \mathbf{n}^f, \quad \text{on} \quad S_i, \tag{3}$$

$$\mathbf{v} \cdot \mathbf{n}^f = -\ddot{\varphi}/g, \quad \text{on} \quad S_f.$$

We note here that the boundary condition specified on S_f is a kinematic condition of the free-surface derived from the *Bernoulli* equation [14], but it vanishes when the free-surface fluctuation is neglected.

Taking spatial integration to *Euler* equations together with the definition of the velocity potential function, we have a relation between the hydrodynamic pressure and the velocity potential function

$$p(\mathbf{x}; t) = -\rho\dot{\varphi} + C(t) \tag{4}$$

where $C(t)$ is a time-dependent constant. In particular, for harmonic fluid motions starting from a state of rest, it vanishes.

4. EQUIVALENT MASSES ADDED TO THE STRUCTURE

We now present the refinement of classical numerical procedure for the added-mass computation. As mentioned earlier for the basic idea of added-mass, we need to start with an abstract hydrodynamic pressure field in the liquid region. So, we transform the previous boundary-value problem (3) into an alternative form expressed in terms of the hydrodynamic pressure:

$$\begin{aligned} \nabla^2 p &= 0, \quad \text{in} \quad \Omega \times (0, t] \\ \partial p/\partial n^f &= \omega^2 p/g, \quad \text{on} \quad S_f, \\ \partial p/\partial n^f &= -\rho \dot{v}_n, \quad \text{on} \quad S_i, \end{aligned} \tag{5}$$

where $\dot{v}_n$ indicates the normal acceleration of the liquid (then for the structure, $\ddot{u}_n = -\dot{v}_n$). In the above formulation, the *Laplace* equation is obtained from the substitution of *Euler* equations into the continuity equation. The converted boundary condition on S_i is obtained by taking time differentiation to the original boundary condition in equation (3) together with the relation (4)

$$\partial p/\partial n^f = \rho \ddot{\varphi}/g. \tag{6}$$

Next, for harmonic fluid motions, we have

$$\ddot{\varphi} = -\omega^2 \dot{\varphi}. \tag{7}$$

Then, finally we arrive at the converted form.

4.1. FINITE ELEMENT APPROXIMATIONS OF ADDED-MASS MATRICES

Applying the weighted residual formulation to equation (5) and using the divergence theorem, we obtain the following variational formulation:

$$\begin{gathered} \text{For given } \ddot{u}_n \in L^2(S_i), \quad \text{find } p \in H^1(\Omega) \text{ such that} \\ \int_\Omega \nabla q \cdot \nabla p \, \mathrm{d}\Omega = \rho \int_{S_i} q \ddot{u}_n \, \mathrm{d}s + \frac{\omega^2}{g} \int_{S_f} qp \, \mathrm{d}s, \quad \forall q \in H^1(\Omega), \end{gathered} \tag{8}$$

where $L^2(S_i)$ is a square-integrable scalar function space over S_i while $H^1(\Omega)$ a *Hilbert* space [15].

For finite element approximations, we express the global finite element approximations p^h, $\ddot{u}_n^h$ and q^h in terms of finite element basis function matrices Φ and the corresponding nodal vectors $\bar{\mathbf{p}}$, $\ddot{\bar{\mathbf{u}}}_n$ and $\bar{\mathbf{q}}$ such that

$$p^h = \Phi_f \bar{\mathbf{p}}, \quad \ddot{u}_n^h = \Phi_s \ddot{\bar{\mathbf{u}}}_n, \quad q^h = \Phi_f \bar{\mathbf{q}}, \tag{9}$$

where the subscripts "f" and "s" refer to the liquid and the structure regions, respectively. Substituting equation (9) into the variational formulation (8), we obtain

$$\tilde{\mathbf{H}} \bar{\mathbf{p}} = \mathbf{B} \ddot{\bar{\mathbf{u}}}_n + \omega^2 \mathbf{m} \bar{\mathbf{p}} \tag{10}$$

with

$$\mathbf{B} = \rho \int_{S_i} \Phi_s^{\mathrm{T}} \Phi_f \, \mathrm{d}s, \quad \tilde{\mathbf{H}} = \int_{\Omega} (\nabla \Phi_f)^{\mathrm{T}} (\nabla \Phi_f) \, \mathrm{d}\Omega, \quad \mathbf{m} = \frac{1}{g} \int_{S_f} \Phi_f^{\mathrm{T}} \Phi_f \, \mathrm{d}s. \tag{11}$$

The second term on the RHS of equation (10) is due to the inclusion of the liquid free-surface fluctuation, but it has been neglected in the classical simplified procedure.

Denoting $\tilde{\mathbf{H}} - \omega^2 \mathbf{m}$ by $\mathbf{H}(\omega)$ and separating finite-element nodes of hydrodynamic pressure $\bar{\mathbf{p}}$ into ones on the liquid–structure interface S_i (denoted by $\bar{\mathbf{p}}_s$) and the rest (denoted by $\bar{\mathbf{p}}_f$), we rewrite equation (10) as

$$\begin{bmatrix} \mathbf{H}_{ss} & \mathbf{H}_{sf} \\ \mathbf{H}_{fs} & \mathbf{H}_{ff} \end{bmatrix} \begin{bmatrix} \bar{\mathbf{p}}_s \\ \bar{\mathbf{p}}_f \end{bmatrix} = \begin{bmatrix} \mathbf{B} & 0 \\ 0 & 0 \end{bmatrix} \begin{bmatrix} \ddot{\bar{\mathbf{u}}}_n \\ 0 \end{bmatrix}. \tag{12}$$

Comment 1. The problem becomes frequency dependent when the free-surface sloshing is included, which leads to the frequency-dependent formulation for added-mass matrices.

After static condensation, the nodal vector $\bar{\mathbf{p}}_s$, of hydrodynamic pressure acting on the structure is given by

$$\bar{\mathbf{p}}_s = \mathbf{H}_s^{-1} \mathbf{B} \ddot{\bar{\mathbf{u}}}_n \tag{13}$$

$$\mathbf{H}_s = \mathbf{H}_{ss} - \mathbf{H}_{sf} \mathbf{H}_{ff}^{-1} \mathbf{H}_{fs}. \tag{14}$$

The next step for the added-matrix is a straightforward application of the principle of virtual work. Referring to Figure 3, let us denote by R_n a virtually equivalent normal force acting on the structure and by δw_n a virtual normal displacement of the structure respectively. Then the virtual work done by R_n in a finite element approximation form is expressed by

$$\delta W = \int_{S_i} \delta w_n R_n \, \mathrm{d}s = \delta \bar{\mathbf{w}}_n^{\mathrm{T}} \{\mathbf{R}_n\}, \tag{15}$$

where $\{\mathbf{R}_n\}$ is finite element load vector to be determined. On the other hand, the virtual work done by hydrodynamic pressure is determined as follows:

$$\delta \mathbf{W} = - \int_{S_i} \delta w_n p_s^h \, \mathrm{d}s$$

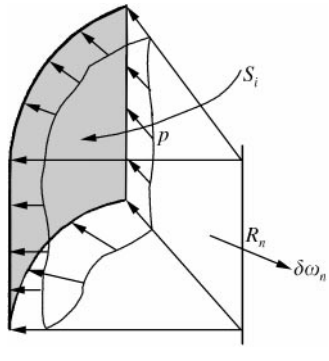

Figure 3. Virtually equivalent normal force $\mathbf{R}_n$ and virtual normal displacement δw_n.

$$
\begin{aligned}
&= -\int_{S_i} (\Phi_s \delta \bar{\mathbf{w}}_n)^{\mathrm{T}} (\Phi_f \bar{\mathbf{p}}_s)\, \mathrm{d}s \\
&= -\delta \bar{\mathbf{w}}_n \left\{ \int_{S_i} \Phi_s^{\mathrm{T}} \Phi_f \, \mathrm{d}s \right\} \bar{\mathbf{p}}_s \\
&= \delta \bar{\mathbf{w}}_n (-\rho^{-1} \mathbf{B}^{\mathrm{T}} \bar{\mathbf{p}}_s),
\end{aligned}
\tag{16}
$$

where we used to symmetry of the matrix $\mathbf{B}$ in equation (11). Equating equations (15) and (16) we have the load vector $\{\mathbf{R}_n\}$ of virtually equivalent normal force given by

$$
\{\mathbf{R}_n\} = -\rho^{-1} \mathbf{B}^{\mathrm{T}} \bar{\mathbf{p}}_s = -\rho^{-1} \{\mathbf{B}^{\mathrm{T}} \mathbf{H}_s^{-1} \mathbf{B}\} \ddot{\bar{\mathbf{u}}}_n. \tag{17}
$$

The application of finite element approximation to the problem (1) yields the usual matrix form of dynamic motion of the structure

$$
[\mathbf{M}] \ddot{\bar{\mathbf{u}}} + [\mathbf{C}] \dot{\bar{\mathbf{u}}} + [\mathbf{K}] \bar{\mathbf{u}} = \{\mathbf{F}_b\} + \{\mathbf{F}_p\}, \tag{18}
$$

where $\{\mathbf{F}_b\}$ and $\{\mathbf{F}_p\}$, respectively, denote load vectors by body force and hydrodynamic pressure. We note here that the load vector $\{\mathbf{F}_p\}$ is constructed in Cartesian co-ordinates while $\{\mathbf{R}_n\}$ in normal co-ordinate. So, we define the co-ordinate transformation operator $\mathbf{T}: R^3 \to R$ such that $\forall \mathbf{v} \in R^3$

$$
\mathbf{T}\mathbf{v} = v_n \in R, \quad \mathbf{T}^{\mathrm{T}}\mathbf{T} = \mathbf{I}. \tag{19}
$$

Then we have

$$
\begin{aligned}
\{\mathbf{F}_p\} &= \mathbf{T}^{\mathrm{T}} \{\mathbf{R}_n\} \\
&= -\rho^{-1} \mathbf{T}^{\mathrm{T}} \{\mathbf{B}^{\mathrm{T}} \mathbf{H}_s^{-1} \mathbf{B}\} \mathbf{T} \ddot{\bar{\mathbf{u}}} \\
&= -\rho^{-1} \mathbf{Q}^{\mathrm{T}} \mathbf{H}_s^{-1} \mathbf{Q} \ddot{\bar{\mathbf{u}}}
\end{aligned}
\tag{20}
$$

with a definition of $\mathbf{Q} = \mathbf{BT}$.

We next add $\{\mathbf{F}_p\}$ to the first term on the left hand side (LHS) of equation (18), then

$$
[\mathbf{M} + \mathbf{M}_{add}] \ddot{\bar{\mathbf{u}}} + [\mathbf{C}] \dot{\bar{\mathbf{u}}} + [\mathbf{K}] \mathbf{u} = \{\mathbf{F}_b\}, \tag{21}
$$

$$
[\mathbf{M}_{add}] = \rho^{-1} [\mathbf{Q}^{\mathrm{T}} \mathbf{H}_s^{-1} \mathbf{Q}](\omega). \tag{22}
$$

Thus, we finally have the numerical procedure for the frequency-dependent added-mass matrix which accounts for the liquid free-surface sloshing.

5. STRUCTURE DEFORMATION ONTO THE LIQUID SLOSHING

For the eigenbehavior analysis of interior liquids, traditionally the structure deformation has been neglected (i.e., the rigid-tank sloshing model). In this section, we present the finite element approximation for the qualitative and quantitative investigation of the effect of structure deformation on the sloshing mode.

For our theoretical study, we start with an alternative form of equation (5) expressed in terms of the velocity potential function:

$$\nabla^2\varphi = 0, \quad \text{in} \quad \Omega\times(0,t],$$
$$\nabla\varphi\cdot\mathbf{n}^f = \begin{cases} -\ddot{\varphi}/g, & \text{on} \quad S_f, \\ \dot{\mathbf{u}}\cdot\mathbf{n}^f, & \text{on} \quad S_i, \end{cases} \tag{23}$$

where the structure deformation is reflected through the boundary condition on the liquid–structure interface S_i. The variational formulation corresponding to the problem (23) is as follows:

$$\text{For given } \dot{u}_n \in L^2(S_i), \text{ find } \varphi \in H^1(\Omega) \text{ such that } \forall\psi \in H^1(\Omega)$$
$$\int_\Omega \nabla\varphi\cdot\nabla\psi \,\mathrm{d}\Omega + \frac{1}{g}\int_{S_f}\ddot{\varphi}\psi \,\mathrm{d}s = \int_{S_i}\dot{u}_n\psi \,\mathrm{d}s. \tag{24}$$

With the previously defined finite element basis function matrices, we express the trial and the test velocity potentials and the structure normal velocity in matrix forms such that

$$\varphi^h = \Phi_f\bar{\varphi}, \quad \dot{u}_n^h = \Phi_s\dot{\bar{\mathbf{u}}}_n, \quad \psi^h = \Phi_f\bar{\psi}. \tag{25}$$

Substituting these approximations into the above problem (24) and separating finite element nodes of the velocity potential in the liquid region into ones (denoted by $\bar{\varphi}_R$) on the liquid free-surface and the rest (denoted by $\bar{\varphi}_I$), we have

$$\begin{bmatrix} \mathbf{M}_{RR} & 0 \\ 0 & 0 \end{bmatrix}\begin{Bmatrix} \ddot{\bar{\varphi}}_R \\ \ddot{\bar{\varphi}}_I \end{Bmatrix} + \begin{bmatrix} \mathbf{H}_{RR} & \mathbf{H}_{RI} \\ \mathbf{H}_{IR} & \mathbf{H}_{II} \end{bmatrix}\begin{Bmatrix} \bar{\varphi}_R \\ \bar{\varphi}_I \end{Bmatrix} = \frac{1}{\rho}\begin{bmatrix} \mathbf{B}_{RR} & \mathbf{B}_{RI} \\ \mathbf{B}_{IR} & \mathbf{B}_{II} \end{bmatrix}\dot{\bar{\mathbf{u}}}_n^*. \tag{26}$$

with the definition of matrices in equation (11) together with

$$\mathbf{M}_{RR} = \frac{1}{g}\int_{S_f}\Phi_f^{\mathrm{T}}\Phi_f \,\mathrm{d}s. \tag{27}$$

In equation (26), the nodal velocity vector $\dot{\bar{\mathbf{u}}}_n^*$ is an extension of $\dot{\bar{\mathbf{u}}}_n$ from the liquid–structure interface to the whole liquid region, hence most components in the enlarged matrix $\mathbf{B}$ are zeros.

In order to correlate $\dot{\bar{\mathbf{u}}}_n$ with the velocity potential, we return to the field equations (1) for the structure region. For the purpose of eigenanalysis, we exclude the damping and the body force terms. Then, the finite element approximation of the eigenbehavior of the structure leads to

$$[\mathbf{M}]\ddot{\bar{\mathbf{u}}} + [\mathbf{K}]\bar{\mathbf{u}} = \{\mathbf{F}_p\}, \tag{28}$$

$$\{\mathbf{F}_p\} = \left(\int_{S_i}\Phi_s^{\mathrm{T}}\Phi_f \,\mathrm{d}s\right)\bar{\mathbf{p}}_s^c = \frac{1}{\rho}\,\mathbf{B}\mathbf{T}^{-1}\bar{\mathbf{p}}_s, \tag{29}$$

where $\bar{\mathbf{p}}_s^c$ is a load vector in Cartesian co-ordinates.

Applying the mass-lumping technique to the mass matrix and separating finite element nodes of the structure displacement into ones on the liquid–structure interface (denoted by $\bar{\mathbf{u}}_n$) and the rest (denoted by $\bar{\mathbf{u}}_c$), equation (28) becomes

$$\begin{bmatrix} \mathbf{K}_{nn} - \omega^2 \mathbf{M}_{nn} & \mathbf{K}_{nc} \\ \mathbf{K}_{cn} & \mathbf{K}_{cc} - \omega^2 \mathbf{M}_{cc} \end{bmatrix} \begin{Bmatrix} \bar{\mathbf{u}}_n \\ \bar{\mathbf{u}}_c \end{Bmatrix} = \frac{1}{\rho} \begin{bmatrix} \mathbf{B} & 0 \\ 0 & 0 \end{bmatrix} \begin{Bmatrix} \mathbf{T}^{-1} \bar{\mathbf{p}}_s \\ 0 \end{Bmatrix}. \tag{30}$$

After static condensation, we have

$$\begin{aligned} \bar{\mathbf{u}}_n &= \rho^{-1} [(\mathbf{K}_{nn} - \omega^2 \mathbf{M}_{nn}) - \mathbf{K}_{nc} (\mathbf{K}_{cc} - \omega^2 \mathbf{M}_{cc})^{-1} \mathbf{K}_{cn}]^{-1} \mathbf{B} \mathbf{T}^{\mathrm{T}} \bar{\mathbf{p}}_s \\ &= \rho^{-1} \mathbf{S}^{-1}(\omega) \mathbf{T}^{\mathrm{T}} \bar{\mathbf{p}}_s. \end{aligned} \tag{31}$$

Using the relation (4) and taking the co-ordinate transformation $\mathbf{T}$ defined earlier, we obtain the nodal vector $\bar{\mathbf{u}}_n$ of the structure part interfacing with the liquid:

$$\bar{\mathbf{u}}_n = -\mathbf{T} \mathbf{S}^{-1}(\omega) \mathbf{T}^{\mathrm{T}} \dot{\bar{\varphi}}_n. \tag{32}$$

Here, $\mathbf{S}^{-1}(\omega)$ denotes $[\cdot]^{-1}\ \mathbf{B}$ on the right-hand-side (RHS) of equation (31).

In order to extend the nodal vectors $\bar{\mathbf{u}}_n$ and $\dot{\bar{\varphi}}_n$ to $\bar{\mathbf{u}}_n^*$ and $\bar{\varphi}$ containing whole finite element nodes in the liquid region, we introduce a matrix operator $\mathbf{D}: S_i \to \Omega$ such that $\forall \bar{\mathbf{a}}_n$ on S_i

$$\mathbf{A} \bar{\mathbf{a}}_n = \mathbf{A} \mathbf{D} \begin{Bmatrix} \bar{\mathbf{a}}_R \\ \bar{\mathbf{a}}_I \end{Bmatrix} \quad \text{and} \quad \mathbf{A} \mathbf{D}^{\mathrm{T}} \begin{Bmatrix} \bar{\mathbf{a}}_R \\ \bar{\mathbf{a}}_I \end{Bmatrix} = \mathbf{A} \bar{\mathbf{a}}_n, \tag{33}$$

where $\mathbf{D}$ is composed of 0 and 1 and $\mathbf{A}$ arbitrary matrix multiplied by $\bar{\mathbf{a}}_n$. Then, we have

$$\dot{\bar{\mathbf{u}}}_n^* = \mathbf{D} \dot{\bar{\mathbf{u}}}_n = -\mathbf{L} \mathbf{S}^{-1} \mathbf{L}^{\mathrm{T}} \begin{Bmatrix} \ddot{\bar{\varphi}}_R \\ \ddot{\bar{\varphi}}_I \end{Bmatrix} \tag{34}$$

where $\mathbf{L} = \mathbf{D}\mathbf{T}$. Substituting $\dot{\bar{\mathbf{u}}}_n^*$ into equation (26) and taking matrix multiplication, we obtain

$$\begin{bmatrix} \mathbf{M}_{RR} & 0 \\ 0 & 0 \end{bmatrix} \begin{Bmatrix} \ddot{\bar{\varphi}}_R \\ \ddot{\bar{\varphi}}_I \end{Bmatrix} + \begin{bmatrix} \mathbf{H}_{RR} & \mathbf{H}_{RI.} \\ \mathbf{H}_{IR} & \mathbf{H}_{II} \end{bmatrix} \begin{Bmatrix} \bar{\varphi}_R \\ \bar{\varphi}_I \end{Bmatrix} = -\begin{bmatrix} \hat{\mathbf{M}}_{RR} & \hat{\mathbf{M}}_{RI} \\ \hat{\mathbf{M}}_{IR} & \hat{\mathbf{M}}_{II} \end{bmatrix} \begin{Bmatrix} \ddot{\bar{\varphi}}_R \\ \ddot{\bar{\varphi}}_I \end{Bmatrix}. \tag{35}$$

From the above equation, we see that the effect of structure deformation is converted to the additional mass matrix $[\hat{\mathbf{M}}]$. Thus, we have the final numerical form describing the flexible-tank sloshing model (as opposed to the classical rigid-tank sloshing model):

$$\begin{bmatrix} \mathbf{M}_{RR} + \hat{\mathbf{M}}_{RR} & \hat{\mathbf{M}}_{RI} \\ \hat{\mathbf{M}}_{IR} & \hat{\mathbf{M}}_{II} \end{bmatrix} \begin{Bmatrix} \ddot{\bar{\varphi}}_R \\ \ddot{\bar{\varphi}}_I \end{Bmatrix} + \begin{bmatrix} \mathbf{H}_{RR} & \mathbf{H}_{RI} \\ \mathbf{H}_{IR} & \mathbf{H}_{II} \end{bmatrix} \begin{Bmatrix} \bar{\varphi}_R \\ \bar{\varphi}_I \end{Bmatrix} = \begin{Bmatrix} 0 \\ 0 \end{Bmatrix}. \tag{36}$$

Comment 2. During the numerical procedure, the displacement boundary condition specified on Γ_D in equation (1) is treated by applying the penalty and penalty method to the stiffness matrix $[\mathbf{K}]$.

Next, we qualitatively analyze the effect of structure deformation on the sloshing mode, to a certain extent. Above all, it is worth noting that the two defined transformations **T** and **D** are magnitude-conserving operators.

Let us compare $\mathbf{M}_{RR}$ defined in equation (27) and $\hat{\mathbf{M}}$ obtained through equations (26)–(35). Neglecting roughly the mass terms in equations (31), due to the low sloshing-mode natural frequencies, together with the definition of **B**, we see that the term (ρ/E) is multiplied in $\dot{\mathbf{u}}_n^*$ (E is the Young's modulus of structures). Thus, referring to the definition of $\mathbf{M}_{RR}$ and two equations, (26) and (31), we recognize that $\hat{\mathbf{M}}$ involves the multiplication of the term $(\rho g/E)$ compared to $\mathbf{M}_{RR}$. For most engineering liquid-storage tanks, this quantity is remarkably small. As an example, for a Ni–Cr steel LNG-storage tank ($E = 7 \times 10^5$ kgf/cm^2 and $\rho g = 4{\cdot}5 \times 10^{-3}$ kgf/cm^3), $\rho g/E$ is of the order of 10^{-8}–10^{-9}.

On the other hand, liquid-storage tanks are ultra-thin structures, so the deformation is approximated well with the classical thin shell theories such as the *Koiter* shell theory. According to thin shell theories [16], the stiffness matrix is split into three; the bending stiffness $\mathbf{K}_b$, the membrane stiffness $\mathbf{K}_m$ and the shear stiffness $\mathbf{K}_s$. The bending stiffness is proportional to h^3 while the other two are proportional to h. Since the deformation behavior in horizontal eigenmotions of structures is bending-dominated, the stiffness matrix **K** is characterized by h^3 even though it is related to the shape, boundary conditions and material properties of structures.

Synthesizing the above arguments, we conclude that the relative magnitude of the converted mass matrix by the structure deformation is related to three major parameters as follows:

$$|\hat{\mathbf{M}}|/|\mathbf{M}_{RR}| \propto (\rho g/E, 1/h^3). \tag{37}$$

Through numerical experiments, we will parametrically investigate the effect of structure deformation on the sloshing mode along with the three parameters ρ, E and h.

6. NUMERICAL EXPERIMENTS

To illustrate the theoretical results discussed so far, we simulated the horizontal vibration problem of a cylindrical tank of uniform thickness h, as shown in Figure 1. The simulation data are given in Table 1, where the three parameters, the Young's modulus E, the liquid density ρ and the structure thickness h are also taken as variables for the parametric investigation.

For the numerical simulation, we developed a test FEM program according to our theoretical results, in which we combined pre- and postprocessor modules of ANSYS commercial FEM software for mesh construction and visualization. We constructed finite

TABLE 1

Material and geometry data for the numerical simulation

	Material data		Geometry data (cm)	
Structure	Density (kgf·s^2/cm^4) (ρ_s)	2·67 ($E-05$)	Radius of tank (R)	2500
	Young's modulus (E) (kgf/cm^2)	7·0 ($E+05$)	Height of tank (H)	4000
	Poisson's ratio (ν)	0·3	Liquid height (H_L)	3000
Liquid	Denisity (kgf·s^2/cm^4) (ρ)	4·6 ($E-06$)	Structure thickness (h)	3

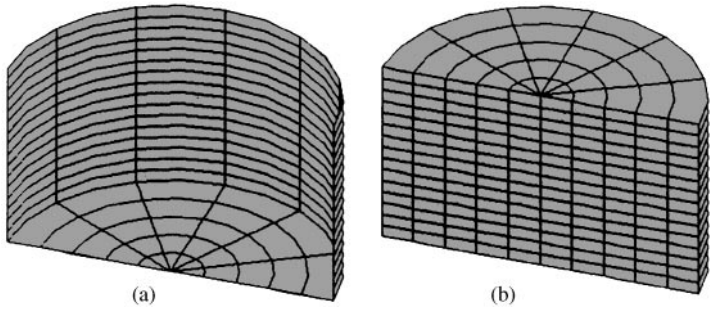

Figure 4. Finite element meshes for the structure and the liquid.

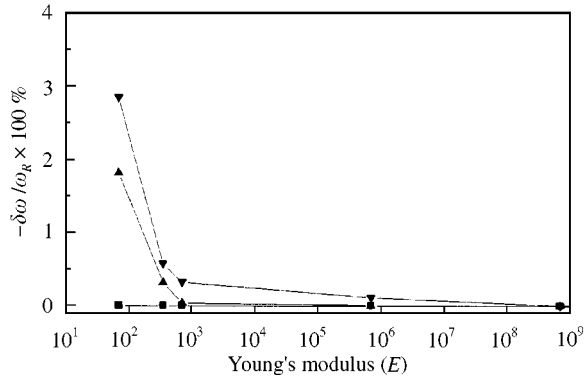

Figure 5. Estimated relative variations in natural frequencies with respect to the Young's modulus. —■—, First mode; —●—, Second mode; —▲—, Third mode; —▼—, Fourth model.

element meshes for the structure and the liquid, as shown in Figure 4, with uniform three-dimensional 20-node cubic and 15-node tetrahedron elements. In particular, for computational convenience in the conversion process of nodal values between two regions, we made the same finite element partition on the common liquid–structure interface. For the computation of natural frequencies and modes, we employed the Lanczos and Jacobi iteration algorithms.

6.1. SLOSHING MODE

Figure 5 shows the relative variations in the lowest natural frequencies with respect to the Young's modulus of structure, where ω_R indicates natural frequencies obtained by the rigid-tank sloshing model and $\delta\omega = \omega_F - \omega_R$. The detailed numerical comparison is contained in Table 2, where the flexible-tank sloshing model produces lower values than those by the rigid-tank sloshing model. The difference between the flexible- and rigid-tank sloshing models becomes considerable as the Young's modulus decreases or the natural frequency increases. In particular we did not experience any noticeable difference in the two lowest eigenmodes within the test range of the Young's modulus and the third and Fourth modes for $E \geqslant 7 \times 10^6$ (kgf/cm^2). Here, we note that the other parameters except for the Young's modulus were assigned the fixed values given in Table 1.

TABLE 2

Variations of natural frequencies with respect to the Young's modulus

Model	Natural frequencies (rad/s)					
	Rigid-tank sloshing model	Flexible-tank sloshing model Young's modulus (kgf/cm^2)				
		7·0e + 01	3·5e + 02	7·0e + 02	7·0e + 05	7·0e + 08
1	0·82091	0·82091 (0%)	0·82091 (0%)	0·82091 (0%)	0·82091 (0%)	0·82091 (0%)
2	1·10484	1·10483 (0%)	1·10484 (0%)	1·10484 (0%)	1·10484 (0%)	1·10484 (0%)
3	1·33340	1·30911 (− 1·822%)	1·32923 (− 0·313%)	1·33382 (− 0·038%)	1·33340 (0%)	1·33340 (0%)
4	1·44509	1·40389 (− 2·851%)	1·43684 (− 0·571%)	1·44054 (− 0·318%)	1·44350 (− 0·110%)	1·44509 (0%)

The parametric effect of the liquid density on the flexible-tank sloshing model is presented in Figure 6 and corresponding numerical data are listed in Table 3. Quite similar variations to the previous results are observed. This is because the density increase implies a relative softening of the structure stiffness.

The relative variations in natural frequencies with respect to the structure thickness are shown in Figure 7, where we observe that its effect on the sloshing mode is not critical compared to the previous two parameters, the Young's modulus and the liquid density. However, for the fourth mode, the variation increases as the thickness decreases (see Table 4).

Figure 8 depicts mode shapes corresponding to the four lowest natural frequencies of the horizontal sloshing motion of interior liquid.

6.2. BULGING MODE

As declared in equation (22), added-mass matrices become frequency-dependent when the liquid free-surface sloshing is taken into consideration. Thus we need a non-linear numerical technique to solve the frequency-dependent bulging mode. Here, we employ a sort of predictor–corrector technique. According to this technique, we first compute natural frequencies $\{\omega_i^{w/o}\}$ corresponding to the bulging mode without free-surface sloshing (i.e., the classical bulging model). For each $\omega_i^{w/o}$, we then compute the corresponding added-mass matrix $[\mathbf{M}_{add}(\omega_i)]$ according to the numerical procedure presented in the previous section. With the computed added-mass matrices, we finally compute the natural frequencies of the bulging mode with free-surface sloshing.

Figure 9 shows the comparative variations of total added mass m_{add}^{TOT} with respect to the natural frequency. Here we see that the case with liquid free-surface sloshing results in smaller total added masses, but the deviation from the case without sloshing diminishes monotonically as the natural frequency becomes higher. This is accordance to the sloshing-height decrease in proportion to the natural-frequency increase, and it implies a weakening in the coupling effect between the liquid free-surface sloshing and the bulging

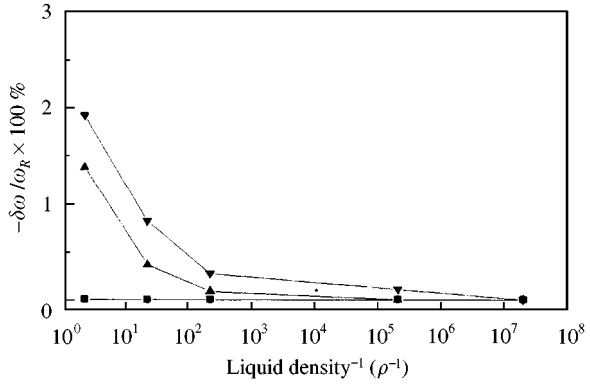

Figure 6. The estimated variations in the four lowest natural frequencies with respect to the liquid density. —■—, First mode; —●—, Second mode; —▲—, Third mode; —▼—, Fourth model.

TABLE 3

Variations of natural frequencies with respect to the liquid density

	Natural frequencies (rad/s)					
		Flexible-tank sloshing model liquid density (kgf s^2/cm^4)				
Model	Rigid-tank sloshing model	4·6e − 08	4·6e − 06	4·6e − 03	4·6e − 02	4·6e − 01
1	0·82091	0·82091 (0%)	0·82091 (0%)	0·82091 (0%)	0·82091 (0%)	0·82091 (0%)
2	1·10484	1·10484 (0%)	1·10484 (0%)	1·10484 (0%)	1·10484 (0%)	1·10484 (0%)
3	1·33340	1·33340 (0%)	1·33340 (0%)	1·33224 (− 0·087%)	1·32854 (− 0·336%)	1·31491 (− 1·387%)
4	1·44509	1·44509 (0%)	1·44350 (− 0·110%)	1·44115 (− 0·273%)	1·43329 (− 0·817%)	1·41735 (− 1·919%)

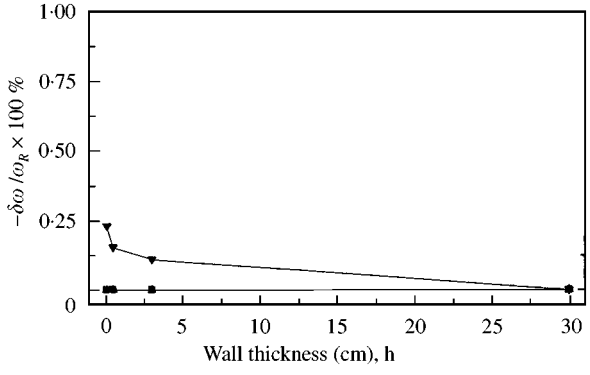

Figure 7. Estimated relative variations in the four lowest natural frequencies with respect to the wall thickness. —■—, First mode; —●—, Second mode; —▲—, Third mode; —▼—, Fourth model.

TABLE 4

Variations of natural frequencies with respect to the structure thickness

Mode	Natural frequencies (rad/s)				
	Rigid-tank sloshing model	Flexible-tank sloshing model structure thickness (cm)			
		0·1	0·5	3·0	30
1	0·82091	0·82091 (0%)	0·82091 **(0%)**	0·82091 (0%)	0·82091 (0%)
2	1·10484	1·10484 (0%)	1·10484 (0%)	1·10484 (0%)	1·10484 (0%)
3	1·33340	1·33340 (0%)	1·33340 (0%)	1·33340 (0%)	1·33340 (0%)
4	1·44509	1·44163 (− 0·239%)	1·44288 (− 0·153%)	1·44350 (− 0·110%)	1·44509 (0%)

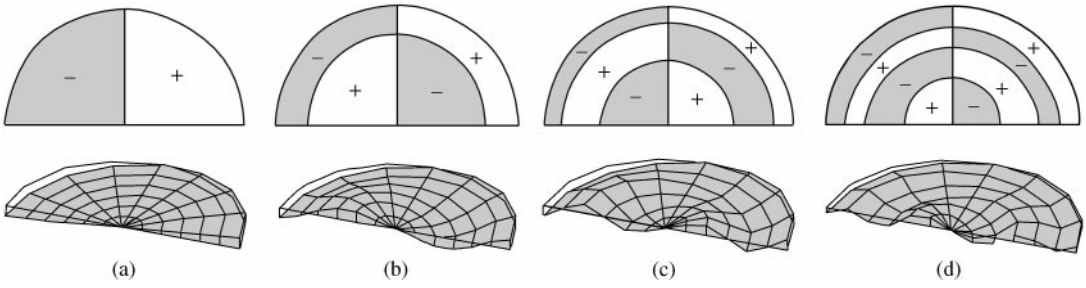

Figure 8. Mode shapes of the horizontal sloshing motion: (a) first mode, (b) second mode,. (c) third mode and (d) fourth mode.

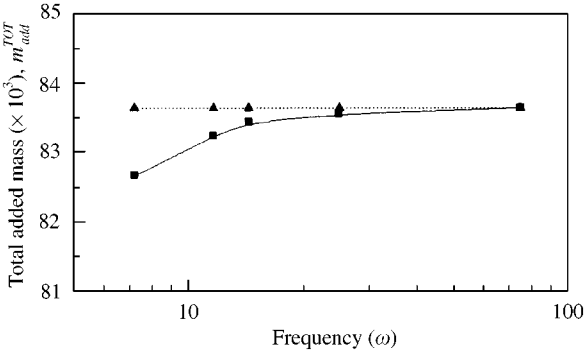

Figure 9. Variations of the computed total added masses with respect to the natural frequency. —■—, with sloshing; ·····▲·····, without sloshing.

mode, as inferred in the eigen-characteristic analysis. On the other hand, by comparing the computed total added masses with the total liquid mass m_{TOT} ($m_{TOT} = \rho\pi R^2 H_L/2 =$ 135 481 kgf s^2/cm), their relative ratios are 61·7% for the case without sloshing and

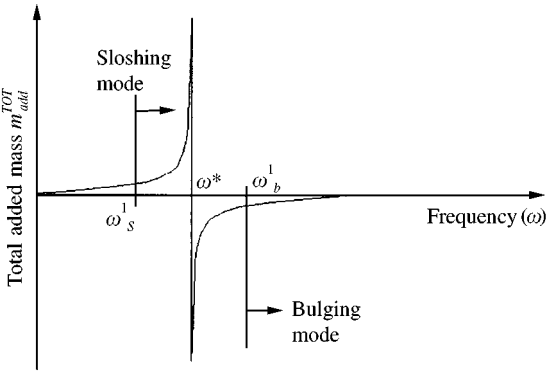

Figure 10. Spectral variation of total added mass along the natural frequency.

TABLE 5

Comparison of natural frequencies of the bulging mode

Mode	Natural frequencies (rad/s)		Relative variation (%)
	W/o sloshing $\omega_b^{w/o}$	With sloshing $\omega_b^{w/}$	
1	7·21646	7·31779	1·405
2	11·65629	11·72005	0·547
3	14·43120	14·45429	0·160

60·7–61·7% for the case with sloshing. It has been reported that the relative ratio of total masses added to the structure increases as the relative liquid height H_L/R increases; however it does not approach 100% but shows a saturation. For more details on the theoretical analysis, the reader may refer to Haroun [4].

Figure 10 presents the spectral variation of total added-mass with respect to the natural frequency for which we computed added-masses by sequentially varying the natural frequency starting from zero. For a reference purpose, actual frequency regions of sloshing and bulging modes of the model tank are indicated. In fact, the added-masses in the frequency region lower than the lowest bulging frequency ω_b^1 do not have physical meaning. However, this plot is to examine the feature of the frequency-dependent matrix $\mathbf{H}_s$ in equation (13). As shown in the figure, we see the singular behavior at $\omega^* = 2{\cdot}263$ rad/s in the sloshing mode region, and it resulted from the singularity of the matrix $\mathbf{H}_s$ near the natural frequency ω^*. This kind of singularity occurs also when one tries to analytically solve the bulging natural frequencies of liquid-storage tanks. A representative example is given in the work by Haroun *et al.* [5].

The comparison of three lowest natural frequencies $\{\omega_b^{w/}\}$ and $\{\omega_b^{w/o}\}$ of the bulging mode between both cases is given in Table 5, where the variation means $(\omega_b^{w/} - \omega_b^{w/o})/\omega_b^{w/o} \times 100\%$. Since a relatively smaller amount of added masses is obtained for the case with the liquid free-surface sloshing, its corresponding natural frequencies are relatively higher. However, the difference between both cases strictly decreases in proportion to the increase of natural frequency. By comparing the numerical results in Tables 2–4 associated with the effect of structure deformation onto the sloshing mode, we recognize the reverse frequency-wise

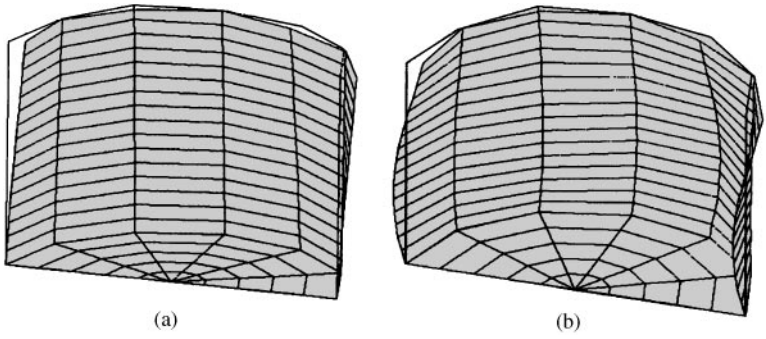

Figure 11. Mode shapes of the two lowest natural frequencies; (a) first mode and (b) second mode.

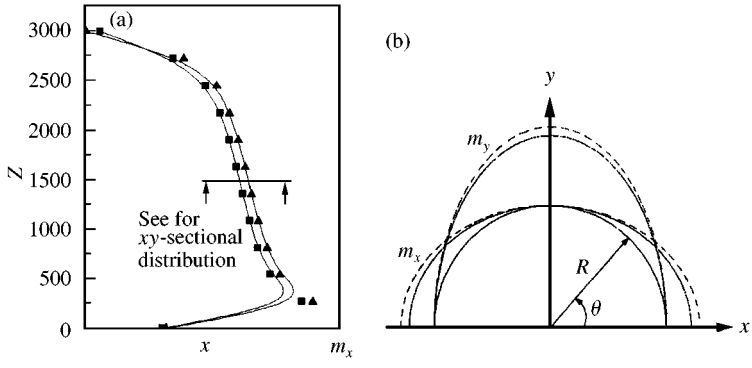

Figure 12. Comparative spatial distributions of component-wise nodal added-masses (for the first lowest bulging mode): (a) aixal —■—, with sloshing; —▲—, without sloshing and (b) xy-sectional – · – · –, with sloshing; ....., without sloshing.

trend; that is, the relative variations in the bulging mode decrease while that in the sloshing mode increases, as the natural frequency increases.

We present the computed mode shapes corresponding to two lowest bulging modes in Figure 11, and we experienced no sensible difference between mode shapes obtained with and without consideration of the liquid free-surface sloshing.

Figure 12 shows the comparative spatial distributions of component-wise nodal added-masses for both cases. The nodal added masses refer to diagonal components in the component-wise lumped added-mass matrix. From Figure 12(a) which shows the axial distributions of the x-component m_x of nodal added-masses (for ω_b^1 and $\theta = 0^\circ$), we see the noticeable difference in the distributions of both cases, particularly at the liquid free-surface. The remarkable difference at the free-surface is directly dependent on whether the liquid free-surface sloshing is taken into consideration or not. From the numerical experiment for different circumferential angles as well as y component m_y, we experienced the same axial distribution pattern for each case, even though the corresponding nodal added-mass magnitudes are different.

On the other hand, Figure 12(b) illustrates the xy-sectional distributions of m_x and m_y at the axial location indicated in Figure 12(a). We note here that no added-mass exists in the z direction according to the inviseid flow assumption.

7. CONCLUSIONS

This paper addressed the assessment of classical simplified dynamic models, the rigid-tank sloshing model and the bulging model without liquid free-surface sloshing, for a convenient eigenanalysis of fluid–structure interaction problems. For this goal, we first refined these simplified models by taking into consideration two neglected effects, the structure deformation on liquid sloshing motions and the liquid free-surface sloshing on structure bulging vibrations.

For the refinement of bulging model, we included the liquid free-surface sloshing into the added mass computation, and for the refined sloshing model we derived the finite element numerical formulation including the structure deformation. According to the refinement, both eigenmodels become frequency dependent.

In order to investigate the additional structure-deformation effect onto the classical rigid-tank sloshing model, we first carried out the qualitative analysis of the refined numerical formulation. We obtained a relation showing the relative variation in added masses that contains three major parameters, the Young's modulus, the liquid density and the structure thickness. Through the parametric experiments for the quantitative variation of sloshing-mode frequencies, the relative difference in natural frequencies between the classical and the refined models prevails in proportion to the relative softening of structures to interior liquids. On the other hand, such a variation becomes remarkable as the natural frequency increases.

With the refined numerical procedure for added-mass matrices, we analyzed the comparative frequency-wise variation of total added mass together with the comparative spatial distributions of component-wise nodal added-masses.

Within the actual bulging-mode frequency range, the total added masses obtained by the refined model are smaller than that by the classical model. However, this difference diminishes with increase in natural frequency while it becomes considerable as the natural frequency becomes lower. Within the sloshing-mode frequency range, the total added mass exhibits a spurious behavior owing to the singularity of the matrix $\mathbf{H}_s$. In accordance with this tendency of the added-mass variations, the refined model leads to relatively higher frequencies compared to the classical model, but the natural frequencies of both models approach each other as the natural frequency becomes higher.

On the other hand, from the comparison of spatial distributions of component-wise nodal added masses, we observed a noticeable difference in axial distributions, particularly at the liquid free- surface.

ACKNOWLEDGMENTS

The financial support for this work by Korea Science and Engineering Foundation under Grant No. 981-1002-016-2 and Agency for Defense Development under contract no. ADD-00-5-6 is gratefully acknowledged.

REFERENCES

1. K. K. GUPTA 1976 *International Journal of Numerical Methods in Engineering* **10**, 637–645. On a numerical solution of the supersonic panel flutter eigen problem.
2. J. F. HALL and A. K. CHOPRA 1982 *Earthquake Engineering and Structural Dynamics* **10**, 333–395. Hydrodynamic effects in the dynamic response of concrete gravity dams.
3. G. W. HOUSNER 1963 *Bulletin of Seismic Society of America* **53**, 381–387. The dynamic behavior of water tanks.

4. M. A. HAROUN 1983 *Earthquake Engineering and Structural Dynamics* **11**, 179–206. Vibration studies and tests of liquid storage tanks.
5. M. A. HAROUN, M. ASCE and M. A. TAYEL 1984 *Journal of Engineering Mechanics* **111**, 346–358. Axisymmetric vibrations of tanks-analytical.
6. O. C. ZIENKIEWICZ and R. L. TAYLOR 1991 *The Finite Element Method*. New York: McGraw-Hill, Fourth Edition.
7. J. W TEDESCO, C. N. KOSTEM and A. KALNINS 1987 *Computers & Structures* **26**, 957–964. Free vibration analysis of cylindrical liquid storage tanks.
8. J. W. TEDESCO, D. W. LANDIS and C. N. KOSTEM 1989 *Computers & Structures* **32**, 1165–1174. Seismic analysis of cylindrical liquid storage tanks.
9. J. RAJASANKAR, N. R. IYER and T. V. S. R. APPARAO 1993 *International Journal for Numerical Methods in Engineering* **36**, 997–1012. A new finite element model to evaluate added mass and for analysis of fluid–structure interaction problems.
10. C. A. BREBBIA, J. C. F. TELLES and I. C. WROBEL 1984 *Boundary Element Techniques*: *Theory and Approximations in Engineering*. Heidelberg: Springer–Verlag.
11. S. L. KHAI 1993 *Journal of Engineering Mechanics* **119**, 1747–1761. Seismic coupled modeling of axisymmetric tanks containing liquids.
12. C. A. CONCA, A. OSSES and J. PLANCHARD 1997 *Computer Methods in Applied mechanics and Engineering* **146**, 387–405. Added mass and damping in fluid–structure interaction.
13. H. J.-P. MORAND and R. OHAYON 1995 *Fluid Structure Interaction–Applied Numerical Methods*. New York: John Wiley & Sons.
14. I. G. CURRIE 1974 *Fundamental Mechanics of Fluids*. New York: McGraw-Hill.
15. J. T. ODEN and L. F. DEMKOWICZ 1996 *Applied Functional Analysis*. Boca Raton, FL: CRC Press Inc.
16. G. WEMPNER 1973 *Mechanics of Solids with Applications to Thin Bodies*. New York: McGraw-Hill.